

# Universality in driven systems with a multiply-degenerate umbilic point

**Johannes Schmidt**

Bonacci GmbH, Robert-Koch-Str. 8, 50937 Cologne, Germany

**Žiga Krajnik**

Department of Physics, New York University, 726 Broadway, New York, NY 10003, United States

**Vladislav Popkov**

Faculty of Mathematics and Physics, University of Ljubljana, Jadranska 19, SI-1000 Ljubljana, Slovenia

Department of Physics, University of Wuppertal, Gaußstraße 20, 42119 Wuppertal, Germany

**Abstract.** We investigate a driven particle system, a multilane asymmetric exclusion process, where the particle number in every lane is conserved, and stationary state is fully uncorrelated. The phase space has, starting from three lanes and more, an umbilic manifold where characteristic velocities of all the modes but one coincide, thus allowing us to study a weakly hyperbolic system with arbitrarily large degeneracy. We then study space-time fluctuations in the steady state, at the umbilic manifold, which are expected to exhibit universal scaling features. We formulate an effective mode-coupling theory (MCT) for the multilane model within the umbilic subspace and test its predictions. Unlike in the bidirectional two-lane model with an umbilic point studied earlier, here we find a robust  $z = 3/2$  dynamical exponent for the umbilic mode. The umbilic scaling function, obtained from Monte-Carlo simulations, for the simplest 3-lane scenario, appears to have an universal shape for a range of interaction parameters. Remarkably, the shape and dynamic exponent of the non-degenerate mode can be analytically predicted on the base of effective MCT, up to non-universal scaling factor. Our findings suggest the existence of novel universality classes with dynamical exponent  $3/2$ , appearing in long-lived hydrodynamic modes with equal characteristic velocities.

PACS numbers:

**Contents**

<b>1</b>	<b>Introduction</b>	<b>3</b>
<b>2</b>	<b>Multilane TASEP: an ideal candidate for studying umbilic modes</b>	<b>4</b>
<b>3</b>	<b>Simulation results</b>	<b>11</b>
3.1	Umbilic universality . . . . .	13
<b>4</b>	<b>Numerical integration of continuous NLFH equations</b>	<b>13</b>
<b>5</b>	<b><math>K &gt; 2</math> case: Universality of umbilic points with higher degeneracy.</b>	<b>15</b>
<b>6</b>	<b>Conclusions</b>	<b>15</b>
 <b>Appendix A</b>		
	Monte-Carlo simulations of a multichain model: dynamic structure factor	17
 <b>Appendix B</b>		
	Numerical simulations of multilane Burgers equations	17
 <b>Appendix C</b>		
	Effective NLFH equations for umbilic mode and comparison with Ref. [17]	18

## 1. Introduction

Systems of driven interacting diffusing particles are paradigmatic models of far from equilibrium dynamics with a broad range of applications in biological, social and physical contexts [4–6]. A coarse-grained (hydrodynamic) description of such models, while smearing out microscopic details, retains the most important properties of the microscopic dynamics such as symmetries and conservation laws. In particular, local conservation laws, under typical assumptions such as locality of interactions, stability of a homogeneous steady state, etc, lead to long-lived slow modes, which show universal (i.e. dependent only on a few crucial properties, such as nonlinearity and locality) behavior at large space-time scales. For instance, one-dimensional driven stochastic systems of particles interacting via short range interactions with a single global conservation law can be mapped to surface growth processes [22] and belong to the renowned KPZ universality class [2]. In case of several conservation laws, the temporal evolution of long-lived modes is described via nonlinear fluctuating hydrodynamics and mode-coupling theory [3].

A cornerstone assumption of nonlinear fluctuating hydrodynamics and mode coupling theory is a spatial separation of modes with time, an assumption referred to as strong hyperbolicity in the theory of hyperbolic conservation laws and hyperbolic shocks [7]. Strong hyperbolicity is crucial for an analysis of hyperbolic shocks, which are, in turn, crucial for understanding intrinsic features of non-equilibrium systems, with no equilibrium counterpart, e.g. boundary-driven phase transitions [4].

At a point in phase space where characteristic velocities of two (or more) modes coincide long-lived modes do not separate in space at long times. Such a point is referred to as an umbilic point (UP), or a point of weak hyperbolicity. Breakdown of the strong hyperbolicity assumption at the UP leads to drastic consequences for temporal dynamics and changes the types of admissible shocks, see e.g. [20, 21].

Universal space-time fluctuations in hyperbolic systems at large scales are also sensitive to the issue of mode separation. While universality properties of space-time fluctuations in strongly hyperbolic systems are relatively well understood, in terms of mode-coupling theory [3], only a few recent studies [16–19] treat universality aspects of the weakly hyperbolic scenario. All these recent studies concern a scenario where a model (either a system of stochastic differential equations, or a driven diffusive particle system) has a single doubly-degenerate umbilic mode, and no other conserved modes exist. While this scenario is undoubtedly basic and minimal, it leaves open some fundamental questions, for instance: (i) How does a degenerate umbilic mode interact with conventional modes? (ii) Can this interaction be described by mode-coupling theory? (iii) What happens in case of a multiple (higher than double) umbilic degeneracy?

In the present communication we, at least partly, clarify the above questions, by considering an interacting particle model with several conservation laws, a multilane totally asymmetric exclusion process. The process is extremely simple and has a

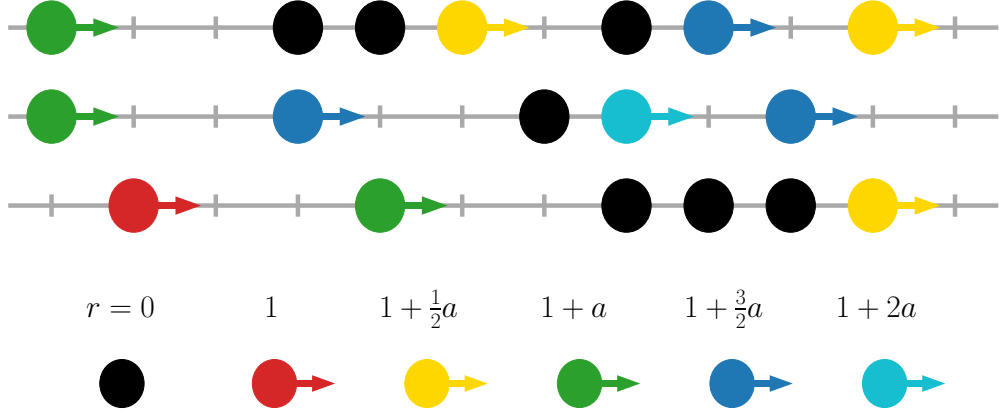


**Figure 1.** Allowable hops for the three-lane model ( $K+1 = 3$ ) with their rates (2.1). Particles with the same color hop with the same rates, e.g. hopping of black-coloured particles is forbidden by hardcore exclusion.

fully uncorrelated steady state, rendering an analytic treatment straightforward and numerical simulations efficient and easy to control. Despite its simplicity, the model supports the existence of umbilic modes of arbitrary degeneracy, and additionally has a single nondegenerate mode, which separates from the umbilic mode with time. In the following, we recall the model's formulation, and investigate stationary density fluctuations of the umbilic mode and of the conventional nondegenerate mode both analytically (via a mode-coupling theory MCT) and numerically (via Monte-Carlo simulations). For the conventional mode, we find an exact correspondence with MCT predictions. For the umbilic mode, our scaling analysis confirms a robust  $z = 3/2$  dynamical exponent, expected from MCT, and a novel family of scaling functions, which depend both on the interaction parameter and on the degree of degeneracy of the umbilic mode.

## 2. Multilane TASEP: an ideal candidate for studying umbilic modes

To observe an umbilic mode, two or more long-lived hydrodynamic modes with coinciding characteristic velocities (respectively, two or more conservation laws) are required. For our study we use a generalization of a totally asymmetric exclusion process (TASEP) to the multi-chain setting, proposed in [15]. The process is illustrated in Fig. 1. In each lane, a particle jumps unidirectionally to the next neighboring site on the same lane with hardcore exclusion; there are  $K+1$  parallel lanes; the rate of hopping depends on local occupation on the other  $K$  lanes as

$$r_k^\lambda = 1 + \frac{a}{2} \sum_{\substack{\mu=1 \\ \mu \neq \lambda}}^{K+1} (n_k^\mu + n_{k+1}^\mu), \quad (2.1)$$

where  $n_k^\mu$  is a occupation number on site  $k$  and lane number  $\mu$  while  $a$  is the interchain interaction. Due to hardcore exclusion sites can be either empty or occupied by one particle,  $n_k^\mu = 0, 1$ . In (2.1) we have chosen a “meanfield” reduction of the multilane TASEP model [15] where a particle in one lane is influenced by neighboring particles in all the other lanes. A continuous time Markov process with rates (2.1) on an infinite lattice has a spatially homogeneous, fully uncorrelated (product measure) steady state, parametrized by set of the average particle densities in each lane  $\{\rho_\mu\}_{\mu=1}^{K+1}$ . The static space correlation matrix in the steady state is

$$K_{\lambda\mu} = \langle n_k^\lambda n_0^\mu \rangle - \rho_\lambda \rho_\mu = \delta_{\lambda\mu} \delta_{k,0} \rho_\lambda (1 - \rho_\lambda). \quad (2.2)$$

In the hydrodynamic limit,  $n_k^\mu(t) \rightarrow \rho_\mu(x, t)$  the system dynamics on the Euler scale is given by a system of continuity equations

$$\frac{\partial \rho_\lambda}{\partial t} + \frac{\partial j_\lambda(\rho_1, \rho_2, \dots, \rho_{K+1})}{\partial x} = 0 \quad (2.3)$$

where  $j_\lambda(\rho_0, \dots) = \langle r_k^\lambda n_k^\lambda (1 - n_{k+1}^\lambda) \rangle$  is the expectation of a particle current on lane  $\lambda$  in the steady state,

$$j_\lambda(\rho_1, \dots, \rho_{K+1}) = \rho_\lambda (1 - \rho_\lambda) \left( 1 + a \sum_{\substack{\mu=1 \\ \mu \neq \lambda}}^{K+1} \rho_\mu \right). \quad (2.4)$$

Nonnegativity of the rates (2.1) implies  $-1/K \leq a < \infty$ . In absence of the interchain interaction  $a = 0$ , the process Fig. 1 splits into  $K + 1$  independent totally asymmetric exclusion processes (TASEPs) characterized by the KPZ universality [1, 2]. For generic interlane interaction  $a \neq 0$  we have  $(K + 1)$  conservation laws (2.3). The characteristic velocities, i.e. velocities of local perturbations over a stationary state with densities  $\rho_\mu$  are given by the eigenvalues of the Jacobian  $J_{\lambda\mu} = \frac{\partial j_\lambda}{\partial \rho_\mu}$ ,

$$J |\lambda\rangle = c_\lambda(\rho_1, \dots, \rho_{K+1}) |\lambda\rangle. \quad (2.5)$$

Interestingly, for an appropriate choice of densities, the multilane model of Fig. 1 with a slight generalization of the rates (2.1) generates a entire discrete set of Fibonacci universality classes [13], with dynamical exponents given by the ratios of nearest Fibonacci numbers  $z_\alpha = 3/2, 5/3, 8/5, \dots$  [13], including the Golden ratio critical exponent. All these cases assume space separation of the long-lived modes with time, meaning that characteristic velocities of all modes are distinct.

Presently, on the contrary, we are looking for umbilic points, i.e. densities  $\{\rho_\mu\}$  for which two or more characteristic velocities  $c_\lambda$  coincide. We find that for the model (2.1) with  $K = 1$  (two-lane system) no umbilic points (UP) exist in phase space of densities, while for any  $K > 1$  a one-parameter UP-containing manifold can be found. Namely, UPs appear whenever the average densities on all lanes become all equal,

$\rho_\lambda \equiv \rho$ : indeed, analyzing the Jacobian  $J_{\mu\lambda}$  we find an umbilic point of order  $K$ , with  $c_1 = c_2 = \dots = c_K \equiv c_u$ ,  $c_{K+1} \equiv c_s$ , where

$$c_u = 1 - 2\rho + a\rho(K - 1 + \rho(1 - 2K)), \quad (2.6)$$

$$c_s = 1 - 2\rho + K a \rho (2 - 3\rho), \quad (2.7)$$

and the lower indices  $u, s$  in the above refer to an umbilic and a single mode respectively. The corresponding single mode eigenvector follows from (2.5)

$$|s\rangle = (1, 1, \dots, 1)^T, \quad (2.8)$$

while eigenvectors of the umbilic modes  $|1\rangle, \dots, |K\rangle$  form a basis in the orthogonal complement of  $|s\rangle$ . Thus for any number of lanes  $K$  we have a line of umbilic points, of order  $K$  (we henceforth refer to it as an umbilic line),  $\rho_\lambda \equiv \rho$ , for any value of interlane interaction  $a$ .

Any infinitesimal shift in the phase space of densities away from the line of equal densities (umbilic line) lifts the degeneracy and makes the system strictly hyperbolic, i.e. all the characteristic velocities  $c_\lambda$  become non-degenerate. Analyzing the behavior of  $c_\lambda$  in an  $\epsilon$ -vicinity of the umbilic line, in any direction orthogonal to the umbilic one, we find for  $K = 2$  an isolated point UP topology, for any value of interaction  $a \neq 0$ , see Fig. 2 for an illustration. (An umbilic point is *isolated* if there exists an  $\epsilon > 0$  such that all of the characteristic velocities  $c_1, c_2, \dots, c_K$  stemming from the umbilic point  $c_1(UP) = \dots = c_K(UP) = c_u$  are different from  $c_u$  in the  $\epsilon$ -vicinity of the UP). For  $K > 2$  umbilic points are no longer isolated, see Fig. 3.

We are interested in the dynamic structure matrix  $\tilde{S}(x, t)$  at the umbilic point  $\rho_\lambda \equiv \rho$  which at large  $x, t$  is expected to exhibit universal behavior. Its components are given by

$$\tilde{S}_{\lambda\mu}(x, t) = \langle e_\lambda | \tilde{S}(x, t) | e_\mu \rangle = \langle n_x^\lambda(t) n_0^\mu(0) \rangle - \rho^2, \quad (2.9)$$

where  $(e_\mu)_\nu = \delta_{\mu\nu}$ . By symmetry we have

$$\tilde{S}_{\lambda\mu} = \begin{cases} \tilde{S} & : \lambda = \mu \\ \tilde{S}' & : \lambda \neq \mu \end{cases} \quad (2.10)$$

We normalize the dynamic structure matrix by rewriting it in the basis of normal eigenmodes, namely by choosing an appropriate transformation  $R$ , such that  $RJR^{-1}$  is diagonal and  $RKR^T = I$  where  $K$  is the covariance matrix (2.2). An appropriate  $R$  is given by the ratio  $R = U/\sqrt{\rho(1 - \rho)}$ , where the rows of the unitary matrix  $U$  are normalized eigenvectors of the Jacobian (2.5) with eigenvalues  $(c_u, c_u, \dots, c_u, c_s)$ . Then

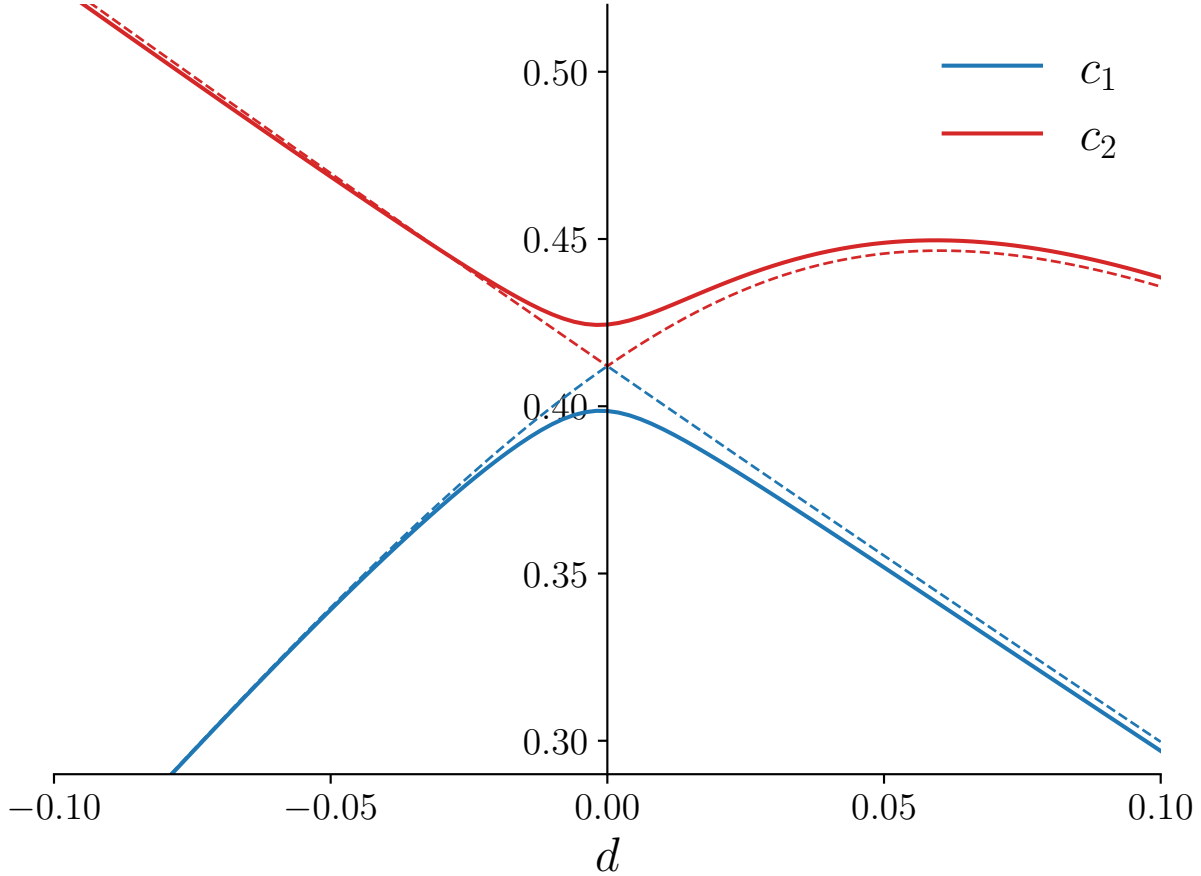


**Figure 2.** Characteristic velocities  $c_1, c_2$ , stemming from the degenerate umbilic mode, along trajectories  $\tilde{\rho}(d)$  in phase space of densities, passing through (or near) the umbilic line, on a manifold orthogonal to it. The parametrization is chosen so that  $d = 0$  corresponds to the minimal distance to the umbilic line. Dashed curves correspond to a trajectory passing through the UP while for solid curves a small mismatch  $\epsilon = 0.005$  is employed. Explicitly, for dashed curves,  $(\rho_1, \rho_2, \rho_3) = (0.3, 0.3, 0.3) + d(1, 1, -2)/\sqrt{6}$  while for solid curves,  $(\rho_1, \rho_2, \rho_3) = (0.3 + \epsilon, 0.3 - \epsilon, 0.3) + d(1, 1, -2)/\sqrt{6}$ . Other parameters:  $K = 2$ ,  $a = 0.4$ . The third characteristic velocity  $c_3$  of the nondegenerate mode is not shown. The curves show the typical topology of an isolated umbilic point, see also the main text.

we have

$$RJR^{-1} = \text{diag}(c_u, c_u, \dots, c_u, c_s), \quad (2.11)$$

$$R\tilde{S}R^T \equiv S = \text{diag}(S_u, S_u, \dots, S_u, S_s), \quad (2.12)$$

$$\text{or } S = S_u(I - |s\rangle\langle s|) + S_s|s\rangle\langle s|, \quad (2.13)$$

$$S_u = \frac{\tilde{S} - \tilde{S}'}{\rho(1 - \rho)}, \quad (2.14)$$

$$S_s = \frac{\tilde{S} + K\tilde{S}'}{\rho(1 - \rho)}, \quad (2.15)$$

where  $S_u$  and  $S_s$  are normalized dynamical structure factors for umbilic and single modes respectively. Denoting by  $\varphi_\lambda(k) = (n_k^\lambda(t) - \rho)$  the density fluctuations on lane  $\lambda$ , the

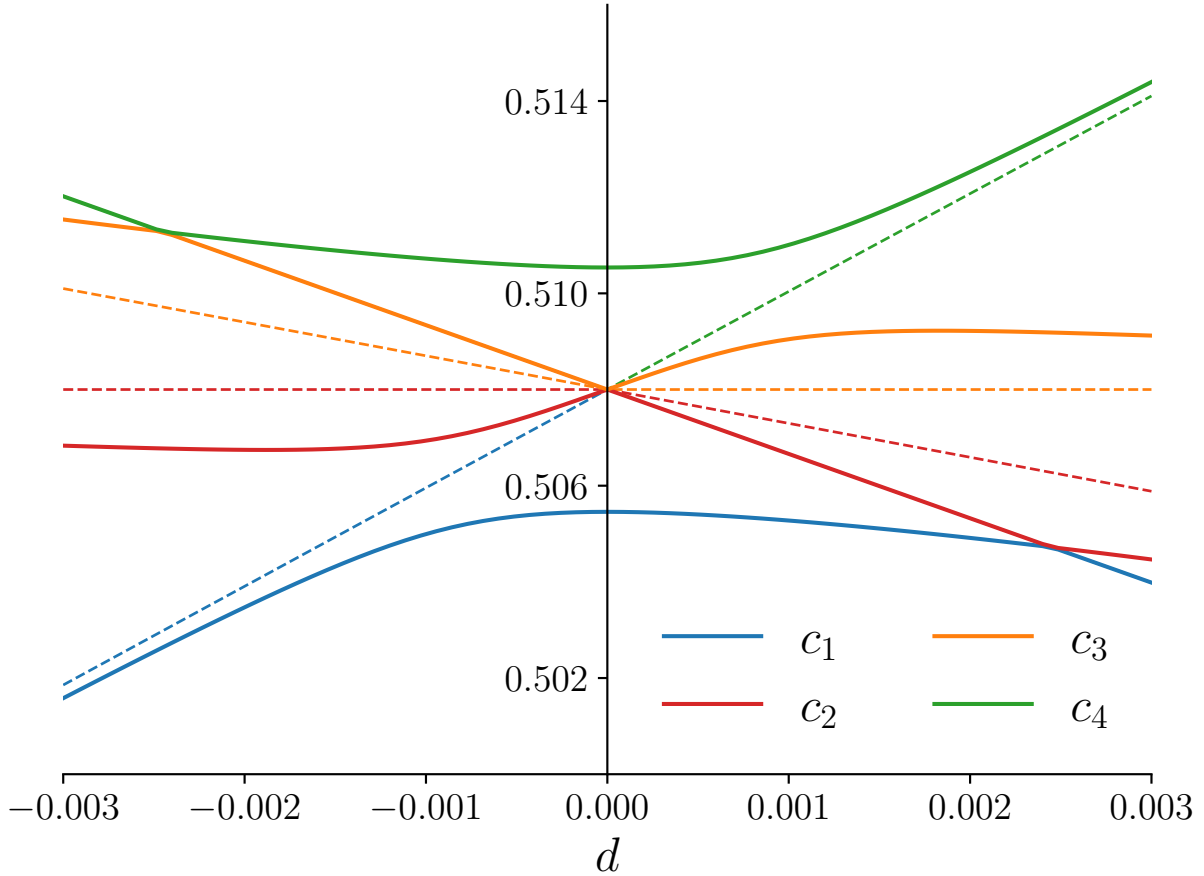


**Figure 3.** Characteristic velocities in the vicinity of an UP with fourfold degeneracy. Two solid curves given by  $\vec{\rho}(\epsilon, d) - (\rho, \rho, \rho, \rho, \rho) = d(1, 1, -2, 0, 0) + \epsilon(0, 0, 0, 1, -1)$  with  $\epsilon = 10^{-3}$  cross the dashed curves  $\vec{\rho}(0, s)$  at the origin, indicating a non-isolated UP. Other parameters:  $K = 4$ ,  $a = 0.4$ ,  $\rho = 0.3$ .

stationary fluctuations  $\phi_\alpha$  of transformed components  $\vec{\phi} = R\vec{\varphi}$  in the hydrodynamic limit  $\phi_\alpha(k) \rightarrow \phi_\alpha(x)$  satisfy canonical relations

$$\langle \phi_\alpha(x) \phi_\beta(0) \rangle = \delta_{\alpha\beta} \delta(x). \quad (2.16)$$

The equations of nonlinear fluctuating hydrodynamics for transformed variables at the UP have the form

$$\partial_t \phi_\lambda = -\partial_x \left( c_\lambda \phi_\lambda + \langle \phi | G^\lambda | \phi \rangle - \partial_x (D\vec{\phi})_\lambda + (B\vec{\xi})_\lambda \right) \quad (2.17)$$

where  $G^\lambda$  is a so-called mode-coupling matrix, describing the effective couplings of normal mode  $\lambda$  to all other modes and to itself [3, 8] while  $B\vec{\xi}$  describes noise and  $D$  is a phenomenological diffusion matrix. The mode-coupling matrices are obtained in usual way

$$G^\alpha = \frac{1}{2} \sum_\beta \tilde{R}_{\alpha\beta} (\tilde{R}^{-1})^T H^\beta \tilde{R}^{-1}, \quad (2.18)$$

where  $\tilde{R} = R/\sqrt{\rho(1-\rho)}$  and  $H^\alpha$  is the Hessian  $(H^\alpha)_{\beta\gamma} = \partial^2 j_\alpha/(\partial\rho_\beta\partial\rho_\gamma)$ .

The long-time evolution of the dynamic structure factors  $S_u, S_s$  at large space-time scales is described by mode-coupling equations

$$\begin{aligned} \partial_t S_\alpha(x, t) &= (-c_\alpha \partial_x + D_\alpha \partial_x^2) S_\alpha(x, t) \\ &+ \int_0^t dt' \int_{-\infty}^{\infty} dx' S_\alpha(x - y, t - t') \partial_y^2 M_{\alpha\alpha}(y, t'), \end{aligned} \quad (2.19)$$

$$M_{\alpha\alpha}(y, t) = 2 \sum_{\beta, \gamma=1}^{K+1} (G_{\beta\gamma}^\alpha)^2 S_\beta(y, t) S_\gamma(y, t) \quad (2.20)$$

where  $S_{n \leq K} = S_u$ ,  $S_{K+1} = S_s$ ,  $D_\alpha$  is the diagonal element of the phenomenological diffusion matrix for the eigenmode  $\alpha$  and  $M_{\alpha\alpha}(x, t)$  is a memory kernel. Due to symmetry in Eq. (2.13) the memory kernel can be written as (omitting variable-dependence for brevity)

$$\frac{1}{2} M_{\alpha\alpha} = \sum_{\beta, \gamma=1}^K (G_{\beta\gamma}^\alpha)^2 S_u^2 + \quad (2.21)$$

$$+ \sum_{\beta=1}^K (G_{\beta, K+1}^\alpha)^2 S_u S_s + (G_{K+1, K+1}^\alpha)^2 S_s^2. \quad (2.22)$$

Summing the above, we obtain the memory kernels

$$\kappa M_{\alpha\alpha} = (K-1)(g_1)^2 S_u^2 + 2(g_2)^2 S_u S_s, \quad (2.23)$$

$$\alpha = 1, \dots, K$$

$$\kappa M_{K+1, K+1} = K(g_1)^2 S_u^2 + (g_3)^2 S_s^2, \quad (2.24)$$

$$\kappa = \frac{K+1}{2\rho(1-\rho)},$$

where  $g_\alpha \equiv g_\alpha(\rho, a)$  are given by

$$g_1(\rho, a) = 1 + a + a\rho(K-2), \quad (2.25)$$

$$g_2(\rho, a) = 1 + a^{\frac{1-K}{2}} + a\rho(2K-1), \quad (2.26)$$

$$g_3(\rho, a) = 1 + aK(3\rho-1). \quad (2.27)$$

Since, due to a symmetry, memory kernels for all umbilic modes  $\alpha = 1, 2, \dots, K$  are equal, the system (2.19) contains just two distinct equations, one for the umbilic mode  $S_u$  with degeneracy  $K$  and another for the single mode  $S_s$ . The system of two equations can be written in terms of effective  $2 \times 2$  mode coupling matrices  $\bar{G}^u \equiv G^1$ ,  $\bar{G}^s \equiv G^{K+1}$

$$\bar{G}^u \equiv \bar{G}^{\alpha \leq K} = \sqrt{\frac{\rho(1-\rho)}{K+1}} \begin{pmatrix} g_1 \sqrt{K-1} & g_2 \\ g_2 & 0 \end{pmatrix}, \quad (2.28)$$

$$\bar{G}^s \equiv \bar{G}^{K+1} = \sqrt{\frac{\rho(1-\rho)}{K+1}} \begin{pmatrix} g_1 \sqrt{K} & 0 \\ 0 & g_3 \end{pmatrix}. \quad (2.29)$$

Here we need to stress that (2.28) and (2.29) are *effective* mode-coupling matrices and respectively (2.19) are *effective* mode-coupling equations, based on symmetries (2.10) occurring at the umbilic manifold. In the effective MCT (2.19),(2.28) the umbilic mode appears as a non-degenerate mode with self-coupling proportional to  $g_1$ . We emphasize that we do expect (2.19) to describe the umbilic mode qualitatively; for the latter purpose we need full system dynamics, captured by e.g. full Monte-Carlo simulations.

Nevertheless, it is instructive to test the predictions of mode-coupling theory for the two effective modes, the umbilic and single mode. According to the scaling hypothesis,  $S_\alpha(x, t)$  at large  $x, t$  has universal scaling behavior

$$S_\alpha(x, t) \simeq (E_\alpha t)^{-1/z_\alpha} f_\alpha \left( (x - c_\alpha t) (E_\alpha t)^{-1/z_\alpha} \right), \quad (2.30)$$

where  $f_\alpha$  is a scaling function,  $z_\alpha$  is a dynamical exponent and  $E_\alpha$  is a non-universal scaling factor. First, note that from non-negativity of the rates (2.1) we have  $-1/K \leq a$  and from (2.25) it follows that

$$\min_{\rho, a} g_1(\rho, a) = \min_\rho \left( 1 - \frac{1 + \rho(K - 2)}{K} \right) = \frac{1}{K} > 0 \quad (2.31)$$

is always positive. Then the degenerate mode (2.28) is a mode with self-coupling,  $\bar{G}_{11}^u \sim g_1 > 0$ . Power counting based on mode-coupling equations yields the standard prediction

$$z_u = \frac{3}{2} \quad (2.32)$$

for the dynamical exponent of the umbilic mode. For the remaining single mode, accounting for  $\bar{G}_{11}^s \sim g_1 > 0$ , two scenarios are possible [12]: (A) if  $\bar{G}_{22}^s \neq 0$  then the single mode is a KPZ mode  $z_s = 3/2$  and  $S_s \equiv f_{\text{KPZ}}$  [2]. (B) if  $\bar{G}_{22}^s \sim g_3 = 0$ , i.e.

$$1 + aK(3\rho - 1) = 0, \quad (2.33)$$

then the Fibonacci universality class [12, 13] criterium predicts

$$z_s = 1 + \frac{1}{z_u} = \frac{5}{3} \quad (2.34)$$

with, additionally, the explicit scaling function  $f_s$

$$f_s(r) = \int_{\mathbb{R}} e^{-E_s |p|^{z_s} [1 - i \cdot \tan(\frac{\pi z_s}{2}) \text{sgn}(p(c_s - c_u))]} e^{ipr} \frac{dp}{2\pi} \quad (2.35)$$

which is a maximally asymmetric Levy stable  $\frac{5}{3}$  distribution. The only free parameter in (2.35) is a nonuniversal scaling factor  $E_s$ , which cannot be predicted from mode-coupling theory [8, 10].

### 3. Simulation results

As stressed after Eq.(2.29), only considering the full dynamics of the system can shed light on the qualitative features on our model, especially for the degenerate umbilic mode. We have performed large-scale Monte-Carlo simulations of the model on Fig. 1 on the umbilic line to test the mode-coupling theory (MCT) predictions. We concentrate on the case (B), i.e.  $g_3 = 0$  in (2.27), which is the most interesting scenario. Our results fully confirmed the validity of the MCT predictions Eqs.(2.32), (2.34), and (2.35), see Figs 4,5.

For the umbilic mode with double degeneracy  $K = 2$  we find an evidence of the dynamic exponent  $z_u = 3/2$  (2.32); however the umbilic scaling function  $f_u$  appears very different from the Prahofer-Spohn (KPZ universality) scaling function. Moreover,  $f_u$  differs from any known scaling function, which can be attributed to  $z = 3/2$  and is symmetric: not only KPZ, but also e.g. Moore-Colaiori function [14], or symmetric Levy stable 3/2 distribution. From our numerical data, we can tabulate  $f_u$  for a doubly degenerate umbilic mode  $K = 2$  with relatively good precision. Remarkably, the shape of the umbilic function is robust to changes of system parameters, i.e. appears universal on the whole umbilic line, see Fig. 6. A possible reason for this universality may be the following: curiously, our umbilic mode considered alone, i.e. ignoring the nondegenerate mode, falls into the umbilic scenario of 2-component systems described in Ref. [17], and can be classified according to it as a special point on a fixed points line, see Appendix C for details. Further confirmation of this reasoning is that, within our numerical precision, the scaling function from continuous time Burgers equation analysis in Ref. [17] match our umbilic scaling function determined from Monte-Carlo simulations, see Fig 4.

As far as the nondegenerate mode is concerned, our findings agree well with mode-coupling theory predictions (2.34), (2.35), see Fig. 5. Note that due to absence of the off-diagonal terms in  $\bar{G}^s$  from (2.29) finite-time effects are small and the Levy stable 5/3 distribution (2.35) is established already for relatively small times. Within our numerical accuracy, starting from times of order  $t = 10^4$  Monte Carlo steps we see no deviations from the analytical result (2.35) apart from a small deviation in the finite-time dynamical exponent. Our findings for the single mode do not depend on the value of interaction  $a$ , as long as the (B) condition  $g_3 = 0$  (2.33) is satisfied.

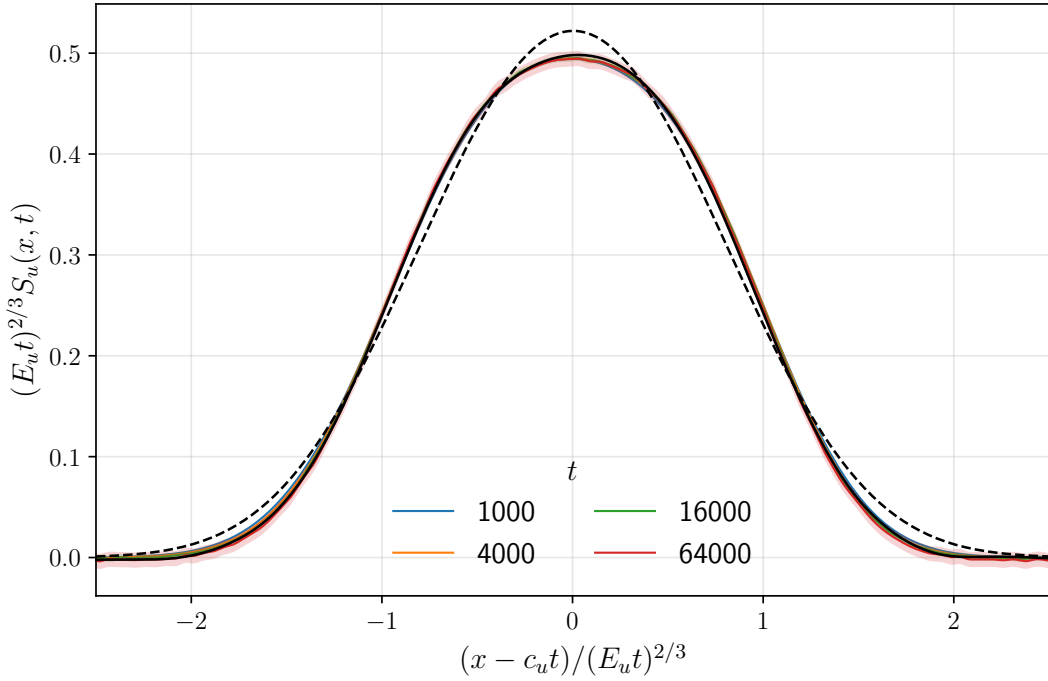


**Figure 4.** Data collapse for the umbilic mode from lattice Monte Carlo simulations with  $z_u = 3/2$ ,  $c_u = 5/8$  and  $E_u = 2.12$ . Shaded regions show two standard deviation neighborhoods. Black curves show the best-fit KPZ (Prähofer-Spohn) scaling function (dashed curve) and the (scaled)  $S_{11}$  correlator of Ref. [17] (full curve) at  $X = Y = -1$ . Simulation parameters:  $K = 2$ ,  $a = 2$ ,  $\rho = 1/4$ , system size  $N = 10^6$ ,  $n_{\text{samples}} = 10^3$ .

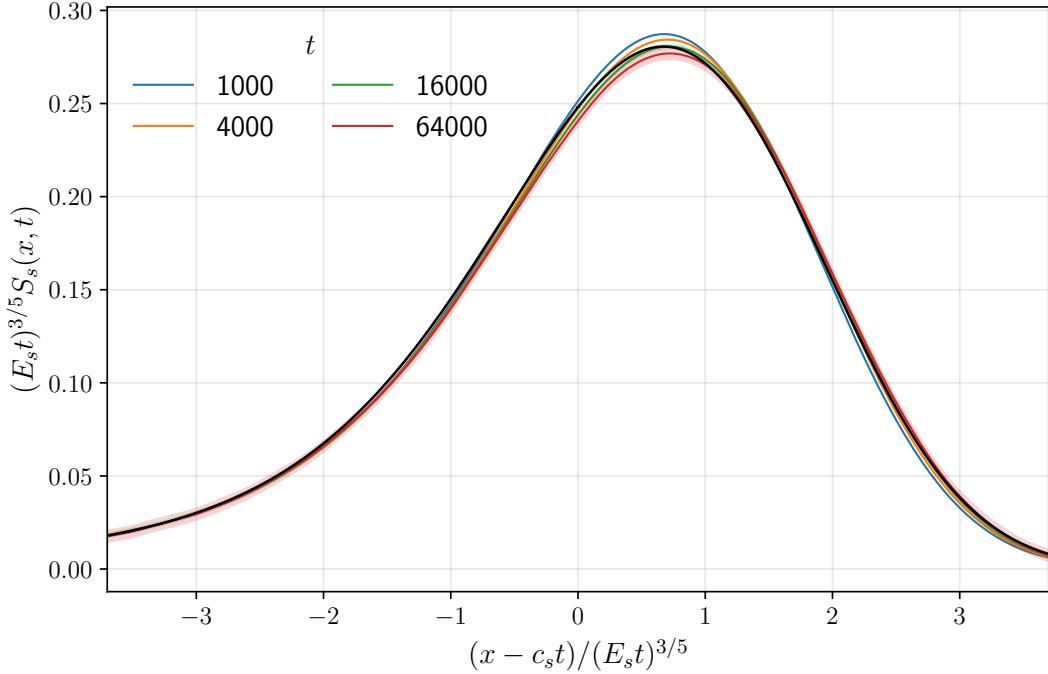


**Figure 5.** Data collapse for the heat mode from lattice Monte Carlo simulations with  $z_s = 5/3$ ,  $c_s = 7/4$  and  $E_s = 1.30$ . Shaded regions show two standard deviation neighborhoods. Best collapse of the data is obtained for  $z_s \approx 1.645$ . Black curve shows the maximally asymmetric Levy stable  $\frac{5}{3}$  distribution (2.35). Simulation parameters as in Fig. 4.

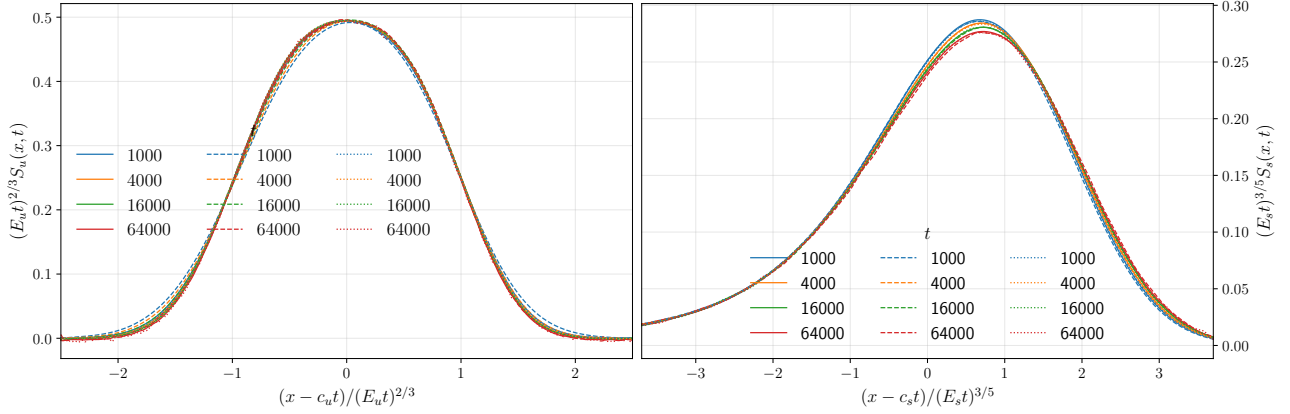


**Figure 6.** Comparison of scaled umbilic (left panel) and heat (right panel) modes from lattice Monte Carlo simulation for  $a = 2$ ,  $\rho = 1/4$  (full curves),  $a = 1$ ,  $\rho = 1/6$  (dashed curves) and  $a = 3$ ,  $\rho = 5/18$  (dotted curves), satisfying the condition (2.33) for the absence of self-coupling. Other simulations parameters as in Fig. 4.

### 3.1. Umbilic universality

We find that the umbilic scaling function does not depend on the interlane interaction parameter for fixed  $K$ , see Fig. 6. In this respect the scaling function appears more robust than the one of a two-lane bidirectional particle model [16, 18] where the umbilic scaling function varies the interlane interaction parameter, called  $\gamma$  in [16, 18].

## 4. Numerical integration of continuous NLFH equations

To check our findings in the lattice model we have also performed an numerical analysis of the stochastic system of equations of nonlinear fluctuating hydrodynamics stemming from the original hydrodynamic equations (2.3), namely,

$$\partial_t \vec{u} = -\partial_x \left( J \vec{u} + \frac{1}{2} \langle u | \vec{H} | u \rangle - \partial_x (D \vec{u}) + (B \vec{\xi}) \right) \quad (4.1)$$

where  $J$  is the Jacobian,  $\vec{H}$  is the Hessian  $(H^\alpha)_{\beta\gamma} = \partial^2 j_\alpha / (\partial \rho_\beta \partial \rho_\gamma)$  and  $u_\alpha(x, t)$  is the deviation of the respective density. Using (2.4), on the diagonal  $\rho_j \equiv \rho$  we have

$$J_{\alpha\beta} = (1 - 2\rho)(1 + K a \rho) \delta_{\alpha\beta} + a \rho(1 - \rho)(1 - \delta_{\alpha\beta}), \quad (4.2)$$

$$\begin{aligned} (H^\alpha)_{\beta\gamma} &= -2(1 + K a \rho) \delta_{\alpha\beta} \delta_{\beta\gamma}, \\ &+ a(1 - 2\rho)(1 - \delta_{\beta\gamma})(\delta_{\alpha\beta} + \delta_{\alpha\gamma}) \end{aligned} \quad (4.3)$$

For  $K = 2$  (three lanes) we have a set of  $K + 1 = 3$  coupled equation, of the form

$$\begin{aligned} \dot{u}_1 &= -\partial_x [du_1 + e(u_2 + u_3) + \frac{1}{2}(fu_1^2 + 2g(u_2 + u_3)u_1) \\ &+ D_1 \partial_x u_1 + B \vec{\xi}_1], \quad \text{etc.} \end{aligned} \quad (4.4)$$

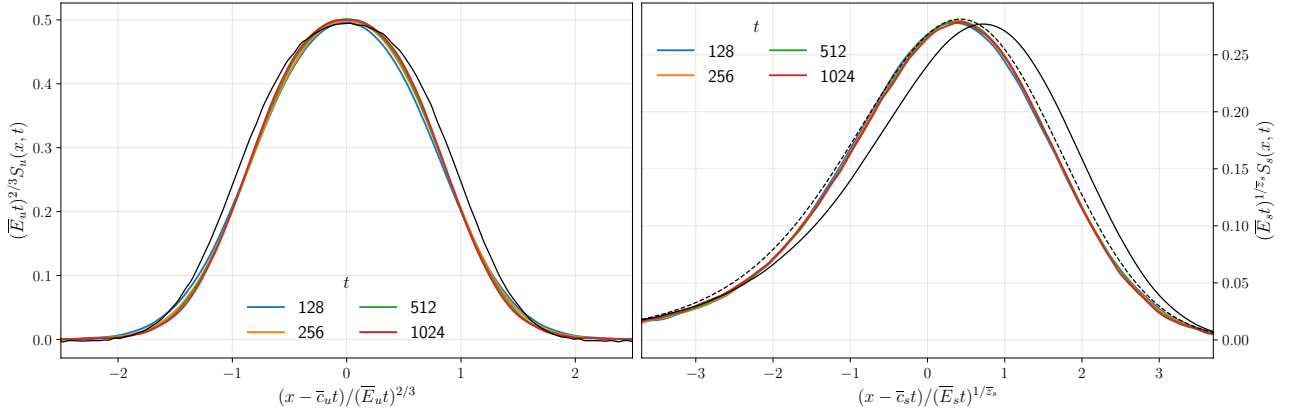


**Figure 7.** Data collapse from continuous NLFH simulation for: (left panel) the umbilic mode with  $\bar{z}_u = 3/2$ ,  $\bar{c}_u = 0.575$  and  $\bar{E}_u = 2.32$ . Black curve shows umbilic scaling function estimated from Monte Carlo simulation for comparison. (right panel) the for heat mode where the best data collapse is obtained for  $\bar{z}_s = 1.74$ ,  $\bar{c}_s = 1.75$  and  $\bar{E}_s = 0.94$ . Black curves show maximally asymmetric Levy stable  $\frac{5}{3}$  (full line) and  $\bar{z}_s$  (dashed line) distributions. Simulation parameters:  $K = 2$ ,  $\rho = 1/4$ ,  $a = 2$  with effective mode-coupling matrices  $\bar{G}^u = \frac{3}{8} \begin{pmatrix} 2 & 1 \\ 1 & 0 \end{pmatrix}$  and  $\bar{G}^s = \frac{3}{8} \begin{pmatrix} 2\sqrt{2} & 0 \\ 0 & 0 \end{pmatrix}$  and discretization parameters  $\Delta t = 2 \times 10^{-3}$ ,  $L = 2^{20}$ .

(the Eqs for  $\dot{u}_2, \dot{u}_3$  are written analogously), where we denoted

$$\begin{aligned} g &= a(1 - 2\rho), & e &= a\rho(1 - \rho) \\ f &= -2(1 + K a \rho), & d &= (1 - 2\rho)(1 + K a \rho), & K &= 2. \end{aligned} \quad (4.5)$$

and the covariance matrix is diagonal,

$$\langle u_\alpha(x), u_\beta(x') \rangle = \rho(1 - \rho) \delta_{\alpha\beta} \delta(x - x'). \quad (4.6)$$

Note that we preferred to integrate the original system of equations rather than the same system after transforming to normal modes (i.e. after diagonalizing the Jacobian) to avoid the ambiguity of the transformation and retain the original symmetry the dynamics. To compare with the Monte-Carlo data of Figs. 4 and 5 we perform the diagonalization to normal modes directly on numerically obtained two-point functions. The results are presented in Fig. 7.

We observe a good agreement in the scaling behavior and shape of the umbilic mode two-point function between lattice Monte Carlo and continuous stochastic PDE simulations. For the heat mode, we find a slight disagreement in scaling (expected scaling  $z_s = 5/3$  in Monte-Carlo simulations, and a slightly different scaling from stochastic PDE simulations), which we attribute to worse convergence properties of the continuous compared to lattice dynamics and non-stationarity of the employed discretization.

### 5. $K > 2$ case: Universality of umbilic points with higher degeneracy.

Up to now we only described our numerical results for the double-degenerate  $K = 2$  umbilic mode, while our effective MCT theory predictions, namely Eqs.(2.32), (2.34), and (2.35) are expected to be valid for an umbilic mode of arbitrary degeneracy  $K$ . We also did a similar analysis for  $K > 2$  which is more challenging numerically, when it comes to Monte-Carlo simulations. While the  $z_u = 3/2$  prediction of MCT (2.32) remains robust, the umbilic scaling function  $f_u$  changes significantly with the umbilic mode degeneracy  $K$ . With increasing  $K$  the umbilic scaling function  $f_u(K)$  starts closely approaching the KPZ scaling function, data not shown. It would be interesting to investigate if the convergence  $f_u \rightarrow f_{\text{KPZ}}$  takes place in the “meanfield” limit  $K \rightarrow \infty$ .

## 6. Conclusions

We have investigated a family of fully asymmetric interacting exclusion processes evolving in parallel on  $K + 1$  lanes, with Bernoulli stationary measure. For  $K \geq 2$  we establish the existence of an umbilic manifold, i.e. a manifold where all but one characteristic velocities coincide. In contrast with another recently investigated umbilic mode scenarios [16–19], here, alongside with the degenerate umbilic mode, a usual nondegenerate long-living mode exist, coupled to the umbilic mode. Concentrating on the umbilic manifold, we investigated the asymptotic behavior of the umbilic mode, which is expected to have universal behavior. We carried out both Monte-Carlo simulations of a particle system on a lattice and simulations of the respective continuity/Burgers-type equations with diffusion and stochastic noise. We found an evidence of a family of universal umbilic structure factors, appearing in asymptotic space-time behavior of a long-lived hydrodynamic modes with equal characteristic velocities (umbilic modes). The umbilic scaling function appears to be symmetric, characterized by the “KPZ” dynamical scaling exponent  $z = 3/2$ , but with a shape distinctly different from the Prahofer-Spohn scaling function [2]. The shape of umbilic function depends on the umbilic degeneracy. We derived effective mode-coupling equations, which describe well some features of our multilane model: in particular, they give a perfect analytic description for the nondegenerate mode, coexisting and interacting with the umbilic mode, for arbitrary degeneracy. On the other hand, an analytic description of the family of umbilic scaling functions at fixed degeneracy, generalizing the Prahofer-Spohn result [2] appears a challenging open problem.

**Acknowledgements** Ž.K. is supported by the Simons Foundation as a Junior Fellow of the Simons Society of Fellows (1141511). V.P. acknowledges support by ERC Advanced grant No. 101096208 – QUEST, and Deutsche Forschungsgemeinschaft through DFG project KL645/20-2. We thank Herbert Spohn and Dipankar Roy for providing the raw scaling function data of Ref. [17].

- [1] M. Kardar, G. Parisi and Y.-C. Zhang, Dynamic scaling of growing interfaces, *Phys. Rev. Lett.* **56**, 889 (1986).
- [2] M. Prähofer and H. Spohn, Exact scaling functions for one-dimensional stationary KPZ growth, *J. Stat. Phys.* **115**, 255–279 (2004).
- [3] H. Spohn, Nonlinear fluctuating hydrodynamics for anharmonic chains, *J. Stat. Phys.* **154**, 1191–1227 (2014).
- [4] G. M. Schütz, in *Phase Transitions and Critical Phenomena*, vol. 19, edited by C. Domb and J. Lebowitz (Academic, London, 2001), doi: 10.1016/S1062-7901(01)80015-X
- [5] D. Mukamel, in *Soft and Fragile Matter: Nonequilibrium Dynamics, Metastability and Flow*, edited by M. E. Cates and M. R. Evans (Institute of Physics Publishing, Bristol, 2000).
- [6] A. Schadschneider, D. Chowdhury and K. Nishinari, *Stochastic Transport in Complex Systems* (Elsevier, Amsterdam, 2010).
- [7] P. D. Lax, *Hyperbolic Partial Differential Equations*, Courant Lecture Notes in Mathematics, vol. 14 (New York, 2000).
- [8] V. Popkov, A. Schadschneider, J. Schmidt and G. M. Schütz, Exact scaling solution of the mode coupling equations for non-linear fluctuating hydrodynamics in one dimension, *J. Stat. Mech.* 093211 (2016).
- [9] J. Baik and E. M. Rains, Limiting distributions for a polynuclear growth model with external sources, *J. Stat. Phys.* **100**, 523 (2000).
- [10] J. Schmidt, G. M. Schütz and H. van Beijeren, A lattice gas model for generic one-dimensional Hamiltonian systems, *J. Stat. Phys.* **183**, 8 (2020).
- [11] H. Spohn and G. Stoltz, Nonlinear fluctuating hydrodynamics in one dimension: The case of two conserved fields, *J. Stat. Phys.* **160**(4), 861–884 (2015).
- [12] V. Popkov, J. Schmidt and G. M. Schütz, Universality classes in two-component driven diffusive systems, *J. Stat. Phys.* **160**(4), 835–860 (2015).
- [13] V. Popkov, A. Schadschneider, J. Schmidt and G. M. Schütz, Fibonacci family of dynamical universality classes, *Proc. Natl. Acad. Sci. USA* **112**, 12645–12650 (2015), DOI:10.1073/pnas.1512261112.
- [14] F. Colaïori and M. A. Moore, *Phys. Rev. E* **65**, 017105 (2001); J. P. Doherty, M. A. Moore, J. M. Kim and A. J. Bray, *Phys. Rev. Lett.* **72**, 2041 (1994).
- [15] V. Popkov and M. Salerno, Hydrodynamic limit of multi-chain driven diffusive models, *Phys. Rev. E* **69**, 046103 (2004).
- [16] D. Roy, A. Dhar, K. Khanin, M. Kulkarni and H. Spohn, Universality in coupled stochastic Burgers systems with degenerate flux Jacobian, *J. Stat. Mech.* 033209 (2024).
- [17] D. Roy, A. Dhar, M. Kulkarni and H. Spohn, Fixed points and universality classes in coupled Kardar-Parisi-Zhang equations, arXiv:2504.04162 (2025).
- [18] J. Schmidt, Ž. Krajnik and V. Popkov, Universality in many-body driven systems with an umbilic point, *J. Stat. Mech.* 083202 (2025).
- [19] H. Spohn, The Popkov-Schütz two-lane lattice gas: Universality for general jump rates, arXiv:2510.12678 (2025).
- [20] G.-Q. Chen and P.-T. Kan, *Arch. Ration. Mech. Anal.* **130**, 231 (1995).
- [21] G.-Q. Chen and P.-T. Kan, *Arch. Ration. Mech. Anal.* **160**, 325 (2001).
- [22] J. Krug, Origins of scale invariance in growth processes, *Adv. Phys.* **46**, 139–282 (1997), <https://doi.org/10.1080/00018739700101498>.
- [23] D. Ertas and M. Kardar, Dynamic roughening of directed lines, *Phys. Rev. Lett.* **69**, 929 (1992).
- [24] E. Medina, T. Hwa, M. Kardar and Y.-C. Zhang, Burgers equation with correlated noise: Renormalization-group analysis and applications to directed polymers and interface growth, *Phys. Rev. A* **39**, 3053 (1989).
- [25] M. Hairer and J. Voss, Approximations to the stochastic Burgers equation, *J. Nonlinear Sci.* **21**, 897–920 (2011), <http://doi.org/10.1007/s00332-011-9104-3>.

## Appendix A.

### Monte-Carlo simulations of a multichain model: dynamic structure factor

Initial states are drawn from the factorized stationary distribution of the process. The two-point function is estimated using translation invariance and stationarity, which allow for the computation of the spatial and temporal averages leading to the Monte-Carlo estimator

$$\tilde{\sigma}_{x,t}^{\lambda\mu}(M, \tau, L) = \frac{1}{LMR} \sum_{l=1}^L \sum_{j=1}^M n_{l+x, j\tau+t}^{\lambda, (r)} n_{l, j\tau}^{\mu, (r)}. \quad (\text{A.1})$$

Finally,  $\tilde{S}_{\lambda\mu}(x, t)$  is obtained by averaging over  $P = n_{\text{sample}}$  independently generated and propagated initial configurations of  $\tilde{\sigma}_{L,x}^{\lambda\mu}$ , i.e.

$$\tilde{S}_{\lambda\mu}(x, t) = \frac{1}{P} \sum_{p=1}^P \tilde{\sigma}_{L,x}^{\lambda\mu, (p)} - \rho_{\lambda} \rho_{\mu} + \mathcal{O}(P^{-1/2}). \quad (\text{A.2})$$

The error estimates for  $\tilde{S}_{\lambda\mu}(x, t)$  are calculated from  $P$  independent measurements, whereas  $L, M, \tau$  are variance reduction parameter.

## Appendix B.

### Numerical simulations of multilane Burgers equations

We seek a numerical scheme that efficiently approximates the solutions of the following system of Burgers equations

$$\partial_t \phi_{\lambda} = \partial_x \left( c_{\lambda} \phi_{\lambda} + \sum_{\alpha, \beta} G_{\alpha\beta}^{\lambda} \phi_{\alpha} \phi_{\beta} + D_{\lambda} \partial_x \phi_{\lambda} + B_{\lambda} \xi_{\lambda} \right). \quad (\text{B.1})$$

We approximate the continuous fields  $\phi_{\lambda}$  by discrete points  $\phi_{x,t}^{\lambda}$  where  $x \in \mathbb{Z}_L$ ,  $t \in \mathbb{Z}$  with spacing 1 and  $\Delta t$  in the spatial and temporal directions respectively. We impose periodic boundary condition by identifying lattices indices as  $L + 1 \equiv 1$ . Along the spatial direction we use the discretization of Ref. [16] while along the temporal direction we adopt a semi-implicit discretization motivated by Appendix A of Ref. [25]. The resulting set of equations reads

$$\sum_y T_{x,y}^{\lambda} \phi_{y,t+1}^{\lambda} = \phi_{x,t}^{\lambda} + \Delta t \mathcal{L}_{x,t}^{\lambda} + \Delta t \mathcal{N}_{x,t}^{\lambda} + (\Delta t)^{1/2} B_{\lambda} (\phi_{x,t}^{\lambda} - \phi_{x-1,t}^{\lambda}) \quad (\text{B.2})$$

where  $T$  is a cyclic tridiagonal matrix ( $\delta$ -function indices are taken modulo  $L$ )

$$T_{x,y}^{\lambda} = (1 + D_{\lambda} \Delta t) \delta_{x,y} - \frac{D_{\lambda} \Delta t}{2} (\delta_{x,y+1} + \delta_{x,y-1}), \quad (\text{B.3})$$

while  $\mathcal{L}$  and  $\mathcal{N}$  are the linear and nonlinear parts of the discretization respectively

$$\mathcal{L}_{x,t}^{\lambda} = c_{\lambda} (\phi_{x,t}^{\lambda} - \phi_{x-1,t}^{\lambda}) + \frac{D_{\lambda}}{2} (\phi_{x+1,t}^{\lambda} - 2\phi_{x,t}^{\lambda} + \phi_{x-1,t}^{\lambda}), \quad (\text{B.4})$$

$$\mathcal{N}_{x,t}^{\lambda} = \sum_{\alpha, \beta} \frac{G_{\alpha\beta}^{\lambda}}{3} \left( -\phi_{x-1,t}^{\alpha} \phi_{x-1,t}^{\beta} - \phi_{x-1,t}^{\alpha} \phi_{x,t}^{\beta} + \phi_{x,t}^{\alpha} \phi_{x+1,t}^{\beta} + \phi_{x+1,t}^{\alpha} \phi_{x+1,t}^{\beta} \right). \quad (\text{B.5})$$

The system (B.2) can be solved efficiently due to the cyclic tridiagonal structure of  $T$ . In particular, using the Sherman–Morrison formula, solving the system (B.2) amounts to solving a pair of tridiagonal systems via the Thomas algorithm.

While the linear part of the spatial discretization (B.4) exactly preserves the dynamics's stationary measure, we emphasize that the nonlinear part of the discretization (B.5) does not. The effects of non-stationarity are suppressed for small time steps  $\Delta t$  and we have checked that for used time steps the deviations from stationarity at longest times, as measured by the static covariance matrix (4.6), are at most a few percent. We note that devising a discretization of the nonlinearity that exactly preserves the stationary measure would facilitate more detailed simulations of the NLFH equations.

## Appendix C.

### Effective NLFH equations for umbilic mode and comparison with Ref. [17]

The NLFH for transformed variables  $\vec{\phi} = R\vec{\varphi}$  at UP have form,

$$\partial_t \phi_\lambda = -\partial_x \left( c_\lambda \phi_\lambda + \langle \phi | G^\lambda | \phi \rangle - \partial_x (D\vec{\phi})_\lambda + (B\vec{\xi})_\lambda \right) \quad (\text{C.1})$$

Because of the degeneracy of the umbilic mode, the diagonalizing transformation  $R$  has a one-parameter freedom. Using a *particular* transformation  $R$  of the form

$$R = (\rho(1 - \rho))^{-\frac{1}{2}} \begin{pmatrix} \frac{1}{\sqrt{2}} & -\frac{1}{\sqrt{2}} & 0 \\ \frac{1}{\sqrt{6}} & \frac{1}{\sqrt{6}} & -\sqrt{\frac{2}{3}} \\ \frac{1}{\sqrt{3}} & \frac{1}{\sqrt{3}} & \frac{1}{\sqrt{3}} \end{pmatrix}, \quad (\text{C.2})$$

we obtain the NLFH equations

$$\partial_t \phi_1 = -\partial_x (c_u \phi_1 + 2b_1 \phi_1 \phi_2 + 2b_2 \phi_1 \phi_3 + D_1 \partial_x \phi_1 + B_1 \xi_1) \quad (\text{C.3})$$

$$\partial_t \phi_2 = -\partial_x (c_u \phi_2 + b_1 (\phi_1^2 - \phi_2^2) + 2b_2 \phi_2 \phi_3 + D_2 \partial_x \phi_2 + B_2 \xi_2) \quad (\text{C.4})$$

$$\partial_t \phi_3 = -\partial_x (c_v \phi_3 + b_1 \sqrt{2} (\phi_1^2 + \phi_2^2) + b_3 \phi_3^2 + D_3 \partial_x \phi_3 + B_3 \xi_3) \quad (\text{C.5})$$

$$\langle \phi_\alpha(x), \phi_\beta(x') \rangle = \delta_{\alpha\beta} \delta(x - x') \quad (\text{C.6})$$

$$b_1 = G_{12}^1 = G_{21}^2 = -\sqrt{\frac{\rho(1 - \rho)}{3}} \frac{1 + a}{\sqrt{2}} \quad (\text{C.7})$$

$$b_2 = G_{13}^1 = G_{31}^1 = -\sqrt{\frac{\rho(1 - \rho)}{3}} \left( 1 + a(3\rho - \frac{1}{2}) \right) \quad (\text{C.8})$$

$$b_3 = G_{33}^3 = -\sqrt{\frac{\rho(1 - \rho)}{3}} (1 + 2a(3\rho - 1)) \quad (\text{C.9})$$

The time-asymptotic form of the umbilic part of the system (C.4) is

$$\partial_t \phi_1 = -\partial_x (c_u \phi_1 + 2b_1 \phi_1 \phi_2 + D_1 \partial_x \phi_1 + B_1 \xi_1) \quad (\text{C.10})$$

$$\partial_t \phi_2 = -\partial_x (c_u \phi_2 + b_1 (\phi_1^2 - \phi_2^2) + D_2 \partial_x \phi_2 + B_2 \xi_2) \quad (\text{C.11})$$

since the products  $\phi_1\phi_3$  and  $\phi_2\phi_3$  become negligibly small due to space separation of the umbilic and single mode. After rescaling time as  $t \rightarrow \tau = b_1 t$ , the reduced system (C.10) becomes

$$\partial_\tau \phi_1 = -\partial_x \left( \frac{c_u}{b_1} \phi_1 + 2\phi_1\phi_2 + D'_1 \partial_x \phi_1 + B'_1 \xi_1 \right) \quad (\text{C.12})$$

$$\partial_t \phi_2 = -\partial_x \left( \frac{c_u}{b_1} \phi_2 + (\phi_1^2 - \phi_2^2) + D'_2 \partial_\tau \phi_2 + B'_2 \xi_2 \right) \quad (\text{C.13})$$

Comparing the above with the classification of umbilic scenarios for 2-component systems of Ref. [17], we find that the system lies on the line of fixed points with

$$X = Y = -1. \quad (\text{C.14})$$

Simulations of umbilic mode in the lattice model show good agreement with this prediction, see Fig. 4.